THE SHAPE OF THE DISK: CLUES FROM THE KINEMATICS OF DISK STARS

MARTIN D. WEINBERG
Department of Physics and Astronomy
University of Massachusetts
Amherst, MA 01003-4525

1. Introduction

It is a tall task to determine the structural parameters of one's own galaxy much less any deviations from axisymmetry. Nonetheless, after hard work, the existence of asymmetries has been reported and discussed in the literature from a wide variety of sources (most recently, Nakai & Nishiyana 1994). Now, in order to understand Milky Way evolutionary history, it is our job to determine the origin and intrinsic structure of these asymmetries.

In the first part of this talk, I will explore the correlation between morphology, pattern speed and kinematics. I will do this using the properties of a particular structure producing mechanism. James Binney has presented arguments for a triaxial halo (this volume). It is worth bearing in mind that one of the main arguments for the existence of the halo was to stabilize the disk (Ostriker & Peebles 1973). Conversely, if the halo itself is not axisymmetric, this will be communicated to the disk. With this motivation, I will demonstrate with a simple model for the Milky Way that a small halo ellipticity may cause a large response in the galactic disk which is remarkably similar to that observed with and features similar to models presented in the literature. More importantly, the generic features of these models corroborate the general finding that pattern speed and kinematics are closely coupled; both the shape of the response and its kinematic signature seem to be insensitive to changes in the amplitude and profile of the perturbation. Although one can already reject some scenarios as unlikely using local kinematic data, many possibilities remain.

In the second part of this talk, I will discuss observational tests, focusing on the importance of stellar kinematics in further discriminating between

L. Blitz and P. Teuben (eds.), Unsolved Problems of the Milky Way, 11–21.

possible dynamical hypotheses. Velocities together with photometric distances play two roles:

1. testing velocity signatures predicted by the dynamical scenarios; and
2. improving, statistically, the photometric distance determinations.

We will discuss each in turn, but the distinction is heuristic; in practice both tasks should be combined. To conclude, I will put both the dynamics and observational tests together and, with a simulation, determine how proposed asymmetry producing mechanisms might be tested.

2. Dynamical scenario

What is the response of the disk to an elliptical halo? Asymmetries on large scales, especially if they originate in the kinematically hot halo/spheroid component, are likely to be smooth and well-represented by low-order harmonic components ($l = 1, 2$ say). If we now insert an axisymmetric stellar disk into this halo it will distort (e.g. Thielheim & Wolff 1984).

To illustrate the response here, I chose a distortion whose scale could be varied, chose a pattern speed, and solved the linearized Boltzmann equation for the response of the disk. For computational ease, I chose a Toomre (1963, Model No. 1) disk with Kalnajs (1976, 1/8 model) analytic distribution function. The resulting model is stable and is a passible fit to the galaxy, although the rotation curve rises a bit slowly from the center and begins to fall past the solar circle (Kalnajs 1976, his Fig. 3). Future work will include a realistic Milky Way profile.

Fig. 1 shows the response of the disk to an elliptical distortion in the halo which peaks near the solar circle, rotated to put the bar in the first quadrant. The y-axis coincides with $l = b = 0°$ in galactic coordinates. The isodensity contours are linearly spaced. Corotation is at roughly 4 kpc; the bar ends inside of this point (≈ 3 kpc); stars orbit clockwise. The peak perturbation is 20% of the initial axisymmetric disk density. The asymmetric features are a forced response; if I slowly removed the halo asymmetry, the bar would go away.

The arrows show the velocity of each standard of rest (SR) relative to circular motion; the largest arrow corresponds to 10 km s^{-1}. Notice that the kinematic major axis is skew to the photometric/density major axis. The small circle marks the position of the Sun. Notice that the Sun sits near an inward radial velocity flow and that the kinematic major axis is skew to the photometric/density major axis. Fig. 2 shows the cut through this diagram along $l = b = 0°$. The trough occurs near the solar position and would result in the outer galaxy appearing to recede at about 8 km s^{-1}, which is only slightly larger and has the same sense as the 6 km s^{-1} as recently measured

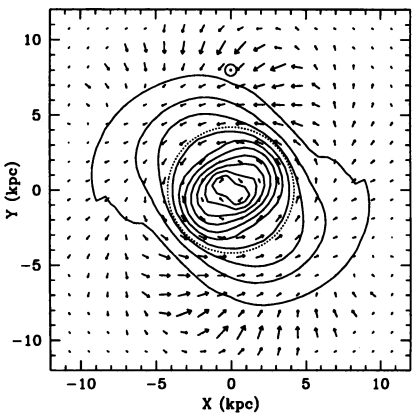

Figure 1. Arrows show velocity of the standard of rest due to fast-pattern bar perturbation. The largest arrow corresponds to $\approx 10\,\mathrm{km\,s^{-1}}$. Contours show the total density including the $m = 2$ perturbation. The dotted line shows the corotation circle and the estimated solar position is indicated ($\odot$).

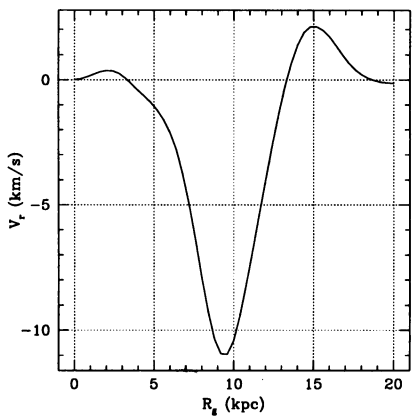

Figure 2. Cut at $l = b = 0°$ for the $m = 2$ perturbation shown in Fig. 1.

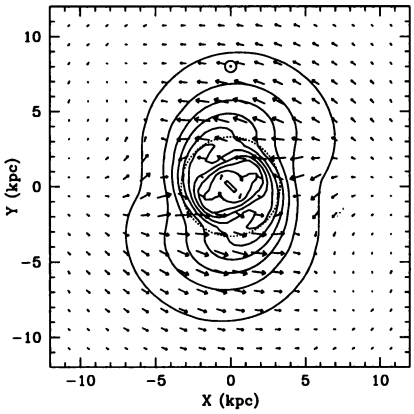

Figure 3. As in Fig. 1 but for a slower pattern speed; the dotted curve now shows the position of the ILR.

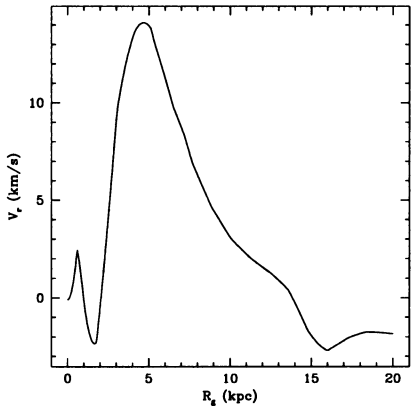

Figure 4. Cut at $l = b = 0°$ for for the slow pattern speed model in Fig. 3.

by Metzger & Schechter (1994) using carbon stars. With no doubt, the measured value could be matched by decreasing the bar amplitude.

https://doi.org/10.1017/S007418090022946X Published online by Cambridge University Press

This general velocity field appears to be a generic signature of a bar with a corotation inside the solar circle. For example, I reported the same trend using a different approach and for a different model (Weinberg 1993). But these features are not obtained for the slowly rotating pattern (e.g. that of a "classical elliptical") shown in Fig. 3. In this case, there is no corotation and the bar now ends at the ILR (which occurs on the rising part of the rotation curve). Compared to Fig. 1, the bar is a bit smaller and the larger scale oval distortion has changed position, but most significantly, the SR velocity field is qualitatively different (Fig. 4). In the slow pattern speed scenario, the LSR is moving outward and from our vantage point the inner galaxy is approaching. Note that there is no first quadrant bar which matches the kinematics (similar lines of argument have been presented by Blitz & Spergel 1992, Kuijken 1992, Kuijken & Tremaine 1994).

The relative orientation and sign of the velocity field relative to the density pattern, appears to be largely independent of the scale of the halo disturbance. Increasing or decreasing this scale by a factor of 1.5 makes very little qualitative difference in the overall features of the response.

For reference, the elliptical distortion in a halo five times more massive than the disk requires an axis ratio of $q = 0.96$ to produce the response seen in Figs. 1 and 3. This "elliptical" would have to be rapidly rotating to match the local kinematics which according to current thinking is unlikely. More generally, this simple scenario suggests that mild halo ellipticity may have dramatic consequences for the disk. For example, if the halo is structured as Binney suggests, the response of the disk provides a probe even if the halo is dark. This issue is far from closed but suggests to me that the connection between the disk and halo is more intimate than implied by the rigid potential invoked to provide the observed rotation curve. Of course, there is the straightforward possibility we are observing an isolated—not externally forced—bar. Clearly what is needed are methods for testing these various hypotheses.

3. Observational tests

In order to probe global structure, one wants to use a tracer that reflects this structure. Although gas is good because it is reactive, for this purpose it can be *too* reactive by responding to small-scale structure. Stars on the other hand are likely to give a fairer picture of the overall gravitational potential. This is illustrated by U- and R- or I-band images of your favorite spiral galaxy (e.g. NGC 4535).

TABLE 1. Candidate tracers

Star	Standard Candle	Tracer
K-giant	poor, $-1 \lesssim V \lesssim 2$ but v. good with metalicity	need low-absorption windows
Cepheid	v. good, v. bright	young pop, in spiral arms
Planetary nebula	fair (20% to 10 kpc)	intermediate pop, systematics?
AGB–OH/IR	fair, bright but $\sigma \sim 1$ mag	inner galaxy/bulge
AGB–Mira/LPV	fair (good if P-L relation)	good, but long-term search
AGB–Carbon	fair→good, $\sigma \sim 0.4$ mag	good, but spectral ID

3.1. TRACER STARS

Table 1 lists the stars most commonly used for kinematic and structural studies with comments on their properties. Although not ideal standard candles because their photometric precision depends on metallicity, K-giants are a work horse. They are plentiful, easily identified spectroscopically and are excellent kinematic targets (see Lewis & Freeman 1989). They are too faint to overcome extinction at small longitudes $|l|$, requiring low-absorption windows; a surmountable but thorny problem for a statistical study. Of all the stars on the list, Cepheids are the best standard candles. Their one disadvantage is their youth; they therefore tend to trace spiral arms and have low scale heights. Planetary nebulae are reported to be fair distance indicators and kinematic targets although systematic effects are still debated in the literature. The last three in Table 1 are the same class of stars, distinguished more by their means of detection. If a period-luminosity relationship holds in the Milky Way as reported for LMC Mira-like stars, the suitability as standard candles improves but this requires a long term search. The carbon stars are bright and with no other information are probably the best tracer among the AGB stars.

3.2. USING VELOCITIES

3.2.1. *Method*

Although, any of the candidates listed in Table 1 might be profitably used, AGB stars are a promising compromise. They are representative of the mixed disk (progenitors have $1\,\mathrm{M}_\odot \lesssim M \lesssim 2\,\mathrm{M}_\odot$) and what they lack as a standard candle can be recovered by either acquiring a larger sample or using velocities. Velocity information refines the distance estimate in much the same way as HI or CO rotation curves are constructed.

The process is depicted in Fig. 5. For this cartoon, we observe an AGB star at longitude $l = 10°$. For a particular rotation curve, the line-of-sight

https://doi.org/10.1017/S007418090022946X Published online by Cambridge University Press

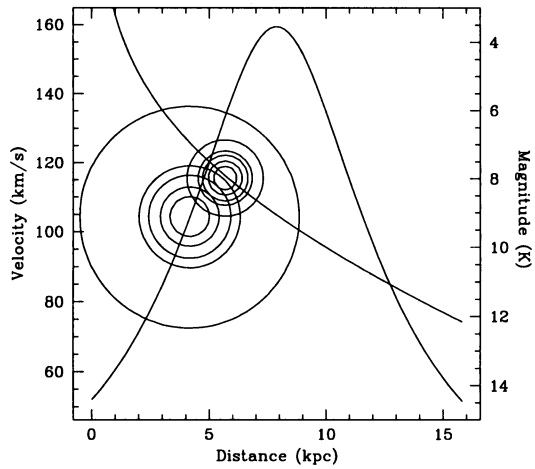

Figure 5. Decreasing curve: m_K vs. distance for an AGB star (right axis). Peaked curve: line-of-sight velocity (v_{los}) vs. distance (left axis). The 50%, 75%, 95% and 99% confidence contours are shown for measured values $v_{los} = 105\,\mathrm{km\,s^{-1}}$ and $m_K = 8$. The joint probability of the two measurements is the product of the two distributions.

velocity is determined as a function of distance (left-hand scale). Similarly, for a given extinction gradient, the apparent magnitude may be computed as a function of distance (right-hand-scale). Assume stars are on circular orbits for argument only. If our model is correct, the star must be at one of the intersections between the two curves. Now, a star is measured with $v_{los} = 105\,\mathrm{km\,s^{-1}}$ and $m_K = 8$ mag. If the velocity measurement error is $10\,\mathrm{km\,s^{-1}}$ and the combined intrinsic dispersion and measurement error for m_K is 0.5, we may compute the joint probability that the star is at either intersection. Not surprisingly, for a gaussian error model, the relative probability that the star is at the closer distance is larger by more than 20 orders of magnitude; this is true for the case depicted in Fig. 5.

For more marginal cases and real world error distributions, there will be considerably less confidence but the lack of symmetry in the two curves gives remarkable statistical leverage. Finally, with many stars and using Bayes theorem, the relative probability of the hypothesis θ is the product of these joint probabilities for each star: $P_{i,\theta} \propto P_{vel}(v_i) \times P_{mag}(m_i)$. The total probability for all stars is then

$$P_{tot} = \prod_i P_{i,\theta}$$

or

https://doi.org/10.1017/S007418090022946X Published online by Cambridge University Press

$$\log L = \sum_i \log P_{i,\theta}. \quad (1)$$

The 'most likely' hypothesis θ maximizes $\log L$: this is the well-known M-L method. For only hundreds of stars, one can do extremely well in estimating parameters, as the following examples will show (see also Schechter et al. 1987).

3.2.2. *Example*

For a simple demonstration, let us estimate the scale length and extinction coefficient from a sparsely selected sample of bright stars ($m_K \leq 6$) with an intrinsic brightness dispersion of $\sigma = 1.0$ mag (this is worse than reality). I assume the galaxy has a flat rotation curve with $V_o = 200\,\mathrm{km\,s^{-1}}$, an exponential disk scale length of 3.5 kpc, $A_K = 0.15$ mags/kpc, and an isotropic velocity ellipsoid with $\sigma = 20\,\mathrm{km\,s^{-1}}$. The photometric and kinematic measurement errors are $\sigma_m = 0.2$ and $\sigma_v = 10\,\mathrm{km\,s^{-1}}$. Fig. 6[1] shows contours of $\log L$ (cf. eq. 1) for different sample sizes. With $N \gtrsim 400$ stars, one has determined the parameters quite well.

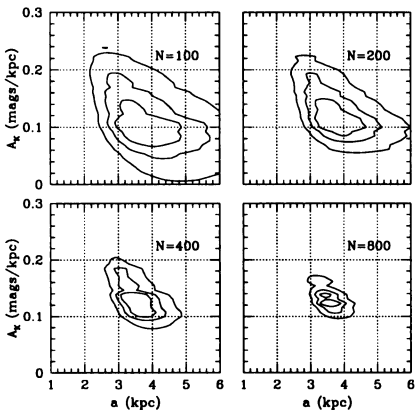

Figure 6. Estimates of scale length and extinction coefficient for different sample sizes. Shown are contours at 75%, 90% and 95% confidence.

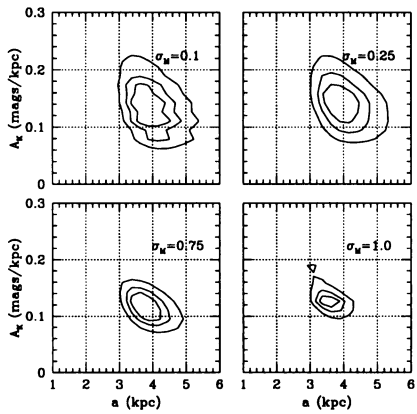

Figure 7. As in Fig. 6 but for various values of σ_M.

A quick aside. Fig. 7 repeats the experiment for $N = 800$ stars but now varies the dispersion of intrinsic tracer star brightness. The confidence improves with *increasing* σ_M. Although somewhat counterintuitive at first

[1]The likelihood surface is often steep; the knotty appearance in some contours is the resulting artifact of the plotting algorithm with an undersampled grid.

https://doi.org/10.1017/S007418090022946X Published online by Cambridge University Press

glance, larger σ_M means that there are brighter stars and therefore more distant probes. As long as the tracer population is distinguishable and well understood, it need not be a high-quality standard candle.

3.3. TESTING DYNAMICAL HYPOTHESES

We now want to compare our dynamical scenarios to real data. In order to do this we need to know the probability function (cf. eq. 1). We may think of Figs. 1 and 3 as the probability that we have a star with a given density from a population with mean velocity relative to the rotation curve shown by the arrows. More precisely, the proper probability function to use is the phase-space distribution function used to make these figures.

Let's look at some examples. Synthetic data sets are easily generated from the theoretical distribution function shown in Fig. 1 whose disturbance has orientation and amplitude 45° and $\epsilon = 0.2$, respectively. Each star is an AGB star with an intrinsic dispersion in magnitude of 0.75 with a standard K-mag extinction gradient. A sparsely-selected flux-limited sample of stars is then "observed" with 5% photometry and $10\,\mathrm{km\,s^{-1}}$ spectroscopic resolution to a limiting magnitude of $K = 10$ (stars at the mean brightness are roughly at the distance of the galactic center). We assume all pattern orientations and positive amplitudes are possible and maximize eq. 1 to determine these parameters.

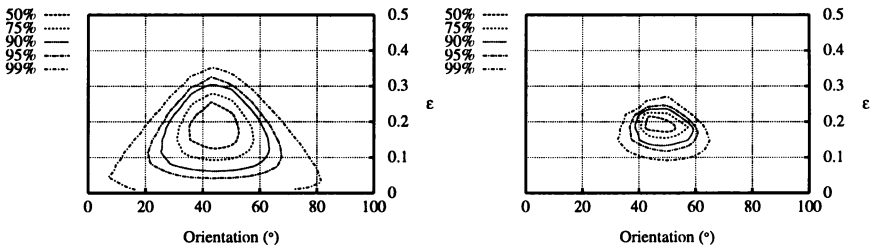

Figure 8. Likelihood contours showing confidence limits on estimates of orientation (in degrees) and bar amplitude (ϵ) and for a simulation with 400 AGB stars and population variance of 0.75 magnitudes. Left: uses photometry only. Right: uses full phase-space distribution.

The M-L estimates based on a sample of 400 stars are shown in Table 2 with 95% confidence error bars (a.k.a. "2–σ"). The likelihood contours are shown in Fig. 8. The panels show the results with photometry only (i, left) and photometry and the full velocity field (ii, right). In case (i), there is a clear detection (zero amplitude is ruled out with 99% confidence) but poor amplitude determination. If I add knowledge of the background rotation curve, the amplitude improves but the estimate of pattern orientation is

https://doi.org/10.1017/S007418090022946X Published online by Cambridge University Press

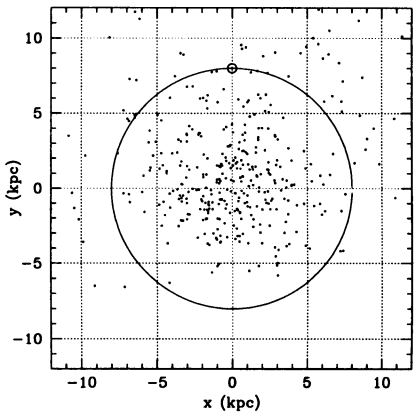

Figure 9. Distribution of AGB stars used in the simulation described by Figs. 8 and 10.

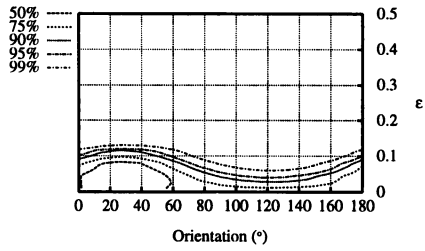

Figure 10. As in Fig. 8 but for slow pattern speed, full phase-space distribution.

TABLE 2. M-L Test Results

Case	Orientation (°)	Amplitude (ϵ)
i	43 ± 15	0.18 ± 14
ii	46 ± 11	0.20 ± 0.07
iii	24 ± 180	0.03 ± 0.05

somewhat worse (not shown). However, using the full distribution function (case ii) improves the estimation dramatically. Should you be unimpressed with the size of the error bars, attempt the estimate by eye from the true distribution of stars on the galactic disk (Fig. 9). With 1200 stars, the estimated orientation and amplitude further improves: $47° \pm 3$ and $0.2^{+0.01}_{-0.05}$. Even with poor standard candles, one can learn about global structure if kinematic information is available.

However, the most useful aspect of this analysis is its power to discriminate between or reject hypotheses. As an example, we can use the same simulated data set to estimate the parameters of the "slow" pattern described in §2 and Fig. 3. One finds that there are no good amplitudes and orientations (Fig. 10). That is, the maximum likelihood solution has amplitude consistent with zero with undetermined position angle. Furthermore, based on the relative values of $\log L$, one can reject the "slow" pattern hypothesis in favor of the the "fast" pattern (case ii) at confidence of 1 part in 10^4.

https://doi.org/10.1017/S007418090022946X Published online by Cambridge University Press

4. Summary

Over the last 10 (and especially 3) years, the textbook picture of the axisymmetric galaxy has faded. The myriad of asymmetries uncovered by observational advances points to the complexity of interactions between structure at different scales and components; the results in §2 are a simple example.

To trace this structure, stars have the advantage of providing both distance and kinematic data simultaneously. In addition, since the information added by the velocity data effectively improves the distance determination, we can tolerate moderate to poor standard candles.

To test the plethora of hypotheses—halo interaction and the more traditional self-consistent disk bar are only a few—I strongly advocate using both spatial and kinematic data together, since the peak signal in their respective fields occur in different places and are sensitive to different parameters (e.g. scale and pattern speed in the case of the $m = 2$ response discussed above). Although there are many possible strategies to this end, the simulations above suggest that a sparsely selected sample $\sim$ 1000 stars with $10\,\mathrm{km\,s^{-1}}$ velocity resolution and limiting K magnitude of 10–12, which roughly penetrates to the galactic center, is sufficient to begin to test some of these dynamical scenarios.

Acknowledgements

I thank the IAU for travel support. This work was supported in part by NASA grant NAG 5-1999 and the Alfred P. Sloan Foundation.

References

Blitz, L. and Spergel, D. N. 1991, Astrophys. J., 370, 205.
Kalnajs, A. J. 1976, Astrophys. J., 205, 751.
Kuijken, K. 1992, Publ. Astron. Soc. Pac., 104, 809.
Kuijken, K. and Tremaine, S. 1994, Astrophys. J., 421, 178.
Lewis, J. R. and Freeman, K. C. 1989, Astron. J., 97, 139.
Metzger, M. R. and Schechter, P. L. 1994, Astrophys. J., 420, 177.
Nakai and Nishiyana 1994, *Radial Distributions of Hα in Barred Galaxies. M83, NGC 4321, NGC 1365, and the Galaxy*, preprint.
Ostriker, J. P. and Peebles, P. J. E. 1973, Astrophys. J., 186, 467.
Schechter, P. L., Aaronson, M., Blanco, V. M., and Cook, K. H. 1987, in L. Blitz and J. Lockman (eds.), *The Outer Galaxy*, pp 31-39, Springer-Verlag.
Thielheim, K. O. and Wolff, H. 1984, Astrophys. J., 276, 135.
Toomre, A. 1963, Astrophys. J., 138, 385.
Weinberg, M. D. 1994, Astrophys. J., 421, 481.

DISCUSSION

P. Schechter: My recollection of the work of Gerhard, Binney and collaborators is that their bar, with a corotation radius of 2.4 kpc produces little kinematic signature at the Sun's position. Is your larger signature the result of your having assumed a larger corotation radius?

Weinberg: Partly; corotation for the fast pattern speed model is nearly 4 kpc. In addition, the self-gravity is to blame for the phase shift between the kinetic and photometric axes, placing the sun near the peak inward velocity. Finally, remember that bar is not self-consistent but a response to a halo ellipticity which is largest near the solar circle.

J. Binney: Can you give some more detail on your bar- in particular, to what radius does your bar's non-axisymmetry rock?

Weinberg: The peak halo asymmetry occurs near the solar circle in both cases presented (fast and slow pattern speeds). Since they are linear solutions, the degree of halo ellipticity depends on the halo to disk mass ratio. For a ratio of 5:1, the axis ratio in the disk plane is Qtrue= 0.96. This value depends on the location of the peak asymmetry; if the location is beyond the solar circle, presumably Qtrue must decrease.

T. de Zeeuw: How sensitive is your method to the assumption of uniform extinction?

Weinberg: It depends on the magnitude of the fluctuation. Variations of $\lesssim$ 1 mag along any line of sight would probably not cause problems. The beauty of this method is that velocities help resolve poor photometric distances. Larger extinction variations can be incorporated as long as they are well characterized a priori. Hopefully, the upcoming infrared surveys will help us do this.